Supplementary material

SM-1 Survey: source and stations.

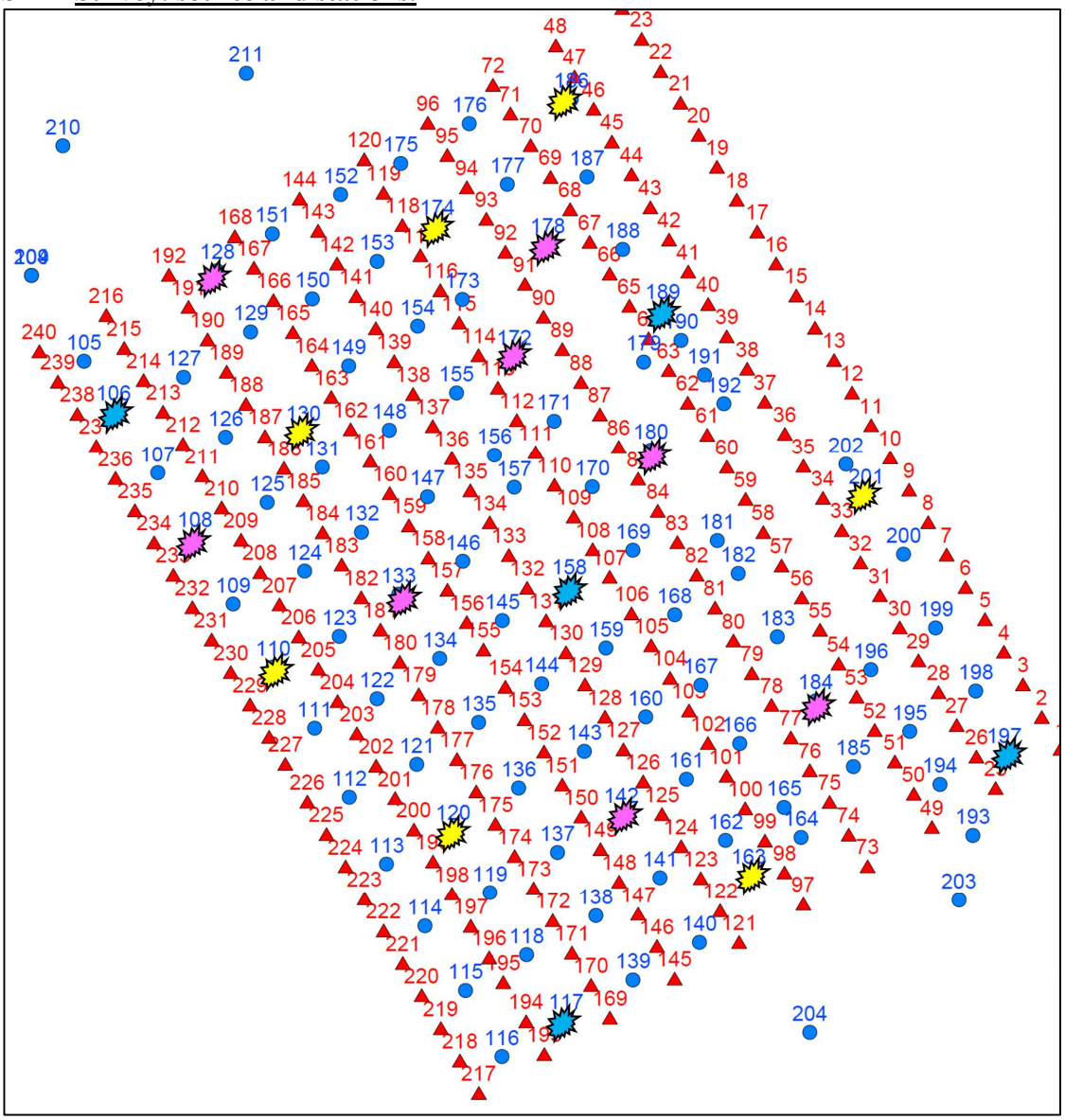

Figure SM-1. *Location of stations (triangles) and events (circles). The 20 sources used in this study are highlighted with the explosion shapes.*

SM-2 Signal analysis

Table SM-2. Inversion controls for each frequency band.

Parameter	**12 Hz**	**18 Hz**	**24 Hz**	**27 Hz**
Frequency Band	8-16 Hz	12-24 Hz	16-32 Hz	18-36 Hz
C/N <3 Coda to Noise Ratio	0.3%	0.3% (=2137 seismograms)	0.09%	0.05%
Outside Peak delay limits (0.3 to 5 s)	3.4%	2.6% (=2081 seismograms available for analysis)	2.5%	2.8%
cc< 0.8 Correlation coefficient for the coda decay method	37.6%	11.3% (=1895 seismograms available for analysis)	2.9%	1.4%
Damping	0.1	0.07	0.05	0.04

Note: Percentages refers to the data discarded

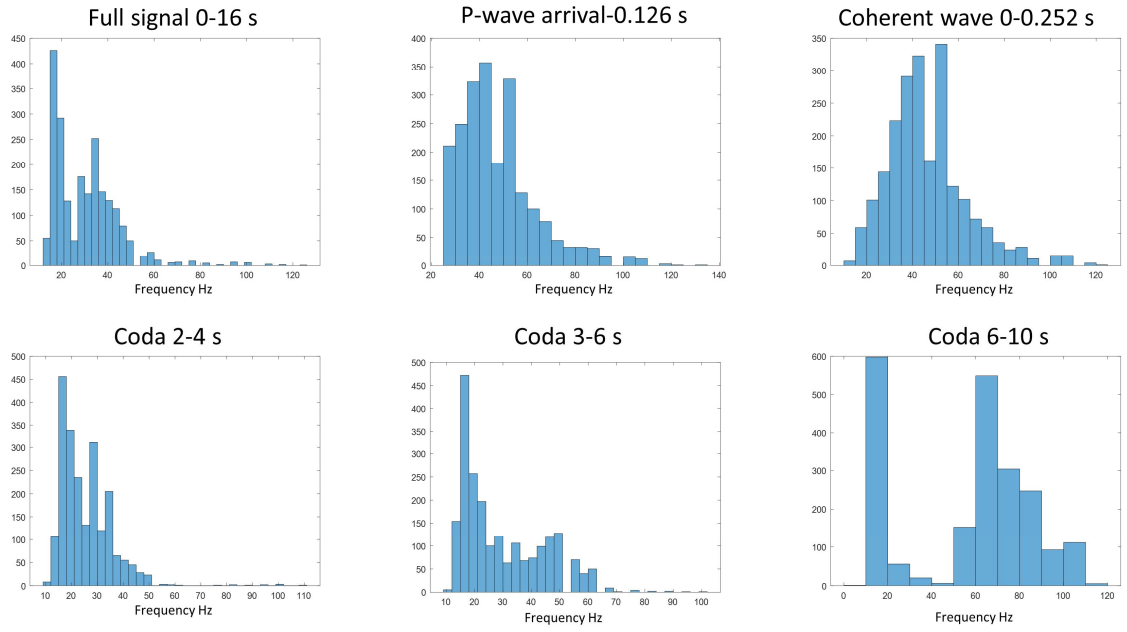

Figure SM-2a. *Histogram of maximum frequency in the spectrum of the unfiltered signal at different windows in time.*

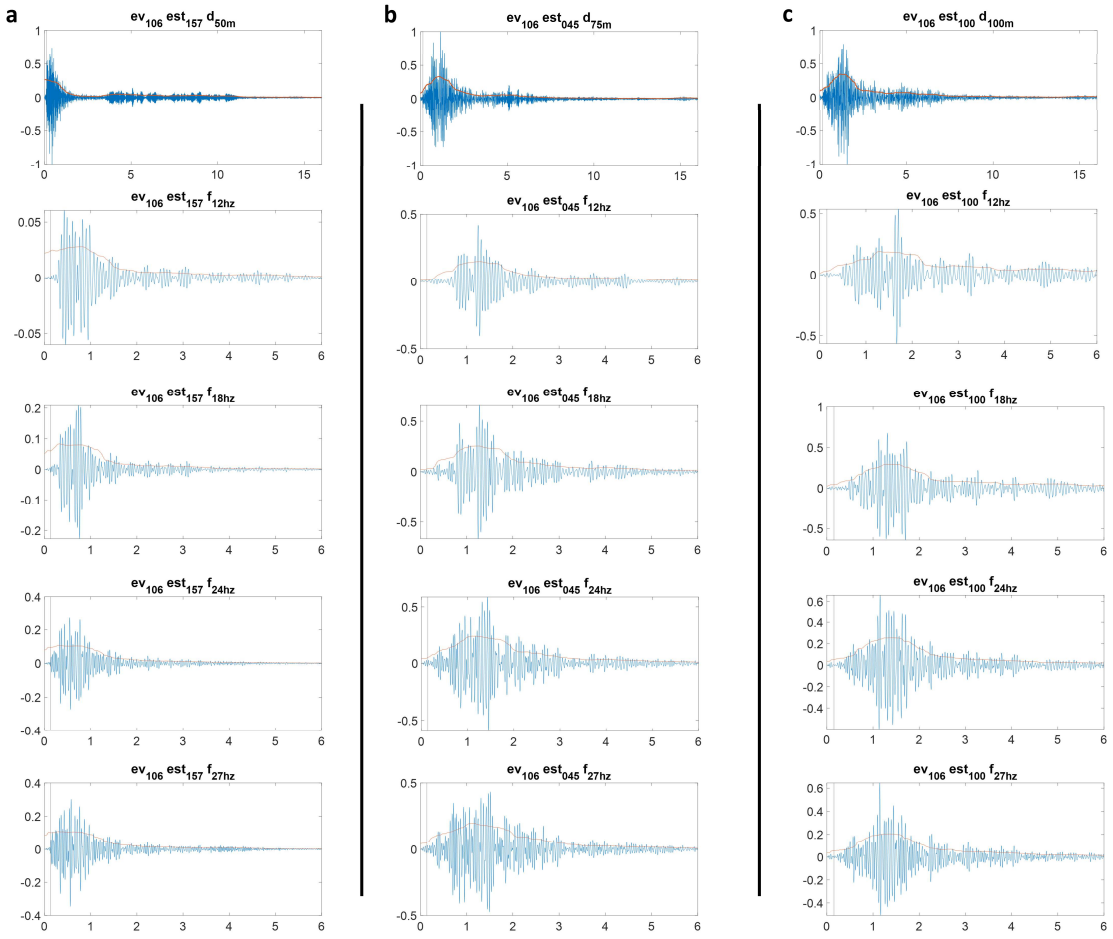

Figure SM-2b. *Example of seismic signals for Source 106 (Figure SM-1) at three stations: 157 (a), 45 (b) and 100 (c) located at ~ 50, 75 and 100 m respectively. The upper panel is the full signal unfiltered, while the rest are filtered at 12, 18, 24 and 27 Hz from top to bottom.*

SM-3 Stability and resolution of the inversion of Coda Attenuation.

Here, we report a mathematical description of the lapse-time-dependent sensitivity kernels for coda attenuation imaging as described by Sketsiou et al., (2020). The energy envelope of the seismogram is defined by Paasschens (1997) using an approximation of the Energy transport equation.

$$E_{i,j}^{3D}[r_{i,j},t] \approx \frac{We^{[-Le^{-1}vt]}}{4\pi r_{i,j}^2 v}\delta\left[t-\frac{r_{i,j}}{v}\right] + WH\left[t-\frac{r_{i,j}}{v}\right]\frac{\left(1-\frac{r_{i,j}^2}{v^2t^2}\right)^{\frac{1}{8}}}{\left(\frac{4\pi vt}{3BoLe^{-1}}\right)^{\frac{3}{2}}}e^{[-Le^{-1}vt]}G[vtBoLe^{-1}\left(1-\frac{r_{i,j}^2}{v^2t^2}\right)^{\frac{3}{4}}]$$

Where $G[s]=e^s\sqrt{1+2.026/s}$; δ and H are the Dirac dental and Heaviside step functions; *W* the source energy; *v* the seismic velocity; and *Bo* and Le^{-1} the albedo and extinction length parameters.

Then the 3D kernels are solved by:

$$K_{i,j}^{3D}[\emptyset,t,Bo,Le^{-1},v]=\int_0^T E^{3D}[r_{s\emptyset},\tau,Bo,Le^{-1},v]E^{3D}[r_{\emptyset r},T-\tau,Bo,Le^{-1},v]d\tau$$

Where ∅ is the space point with coordinates {i,j,z}, $r_{s\emptyset}$ and $r_{\emptyset r}$ are the point to source and -receiver distance, respectively. The steps taken to obtain Bo and Le^{-1} follows Wegler (2003):

1. We filter the seismograms in the frequency range 12-36 Hz using a Butterworth bandpass filter;
2. We compute the envelope of the energy signal for each seismogram *W(r,t)*;
3. We choose the analysis window at time *t* with starting point one sample after the S-wave arrival time and a 9 seconds length;
4. We find the least square solution that fits the following equation
$$log\left[t^{\frac{3}{2}}W(r,t)\right]=a_1+a_2t+a_3\frac{1}{t}$$
where a_2=-*b* is the coefficient of intrinsic attenuation; $d=-r^2/4*a_3$ is the diffusivity, *and* here *r* is the source-receiver distance.
5. We compute the scattering mean free path as *mfp=3*d/Vs*
6. We filter the data to satisfy the assumption *mfp < r/10*, then we compute the attenuation coefficients $n_s=1/mfp$ and $n_i=b/Vs$
7. Finally, albedo and extinction length are $Bo=\frac{n_s}{(n_i+n_s)}$ and $Le=\frac{1}{(n_i+n_s)}$, respectively.

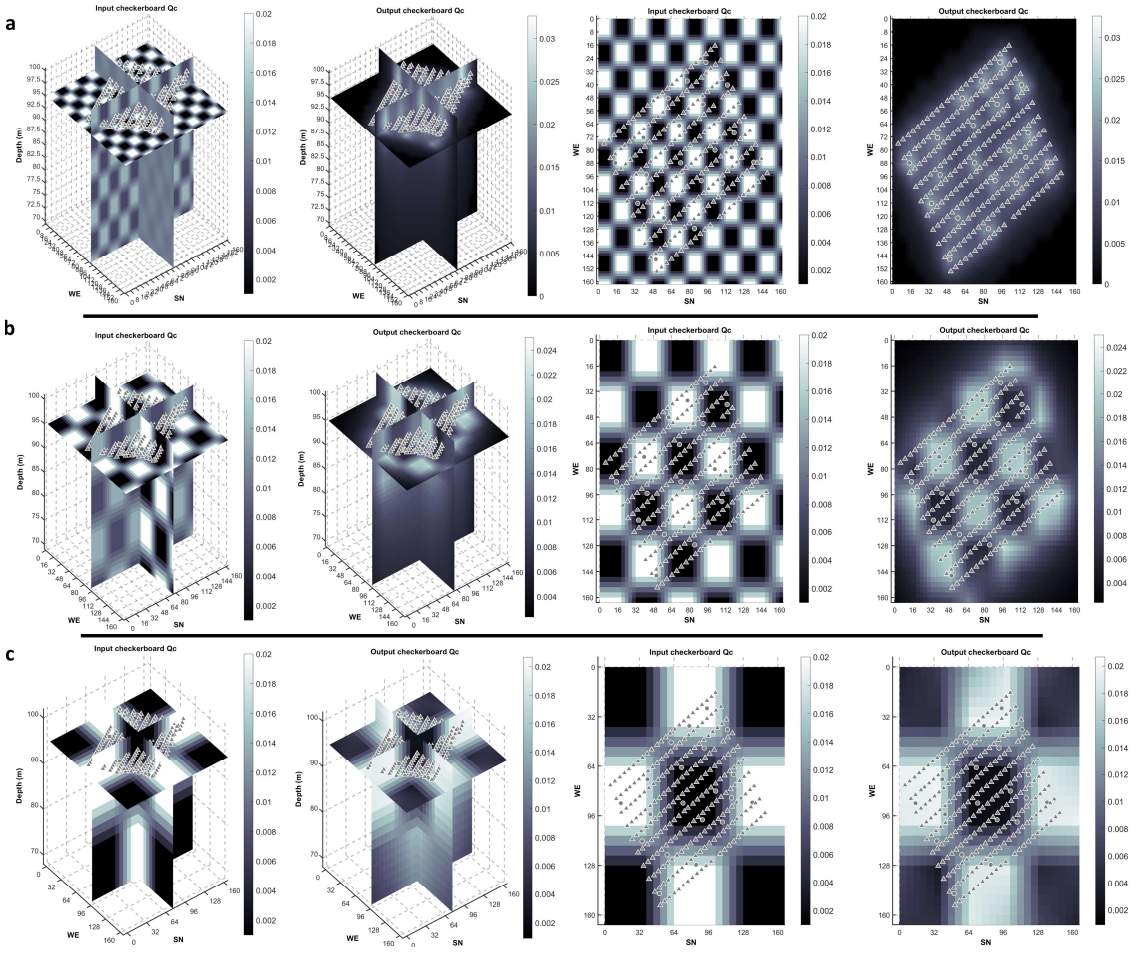

Figure SM-3a. *Checkerboard test for the inversion performed at 18 Hz and three different node parameterizations: (a) 21x21x13;(b) 11x11x7; (c) 6x6x4. The results in the manuscript correspond to panel (b). Note that for the parameterization of panel (a) the anomalies are not well reconstructed, while for panel (b) the sign and location of the anomalies are retrieved in the area occupied by the stations; the output of panel (c) is well resolved laterally but does not represent an improvement in the inversion (see Picard plot in Figure SM-3b). The depth slices (right panels) are at 95 m. The resolution at depth is only reliable in the first 10 m, below this depth it is not possible to resolve the anomalies because the sensitivity kernels (Figure SM-3c) used in this analysis depend on the source-station locations. Given that sources are located at the surface it is not possible to go deeper into the resolution of the coda results.*

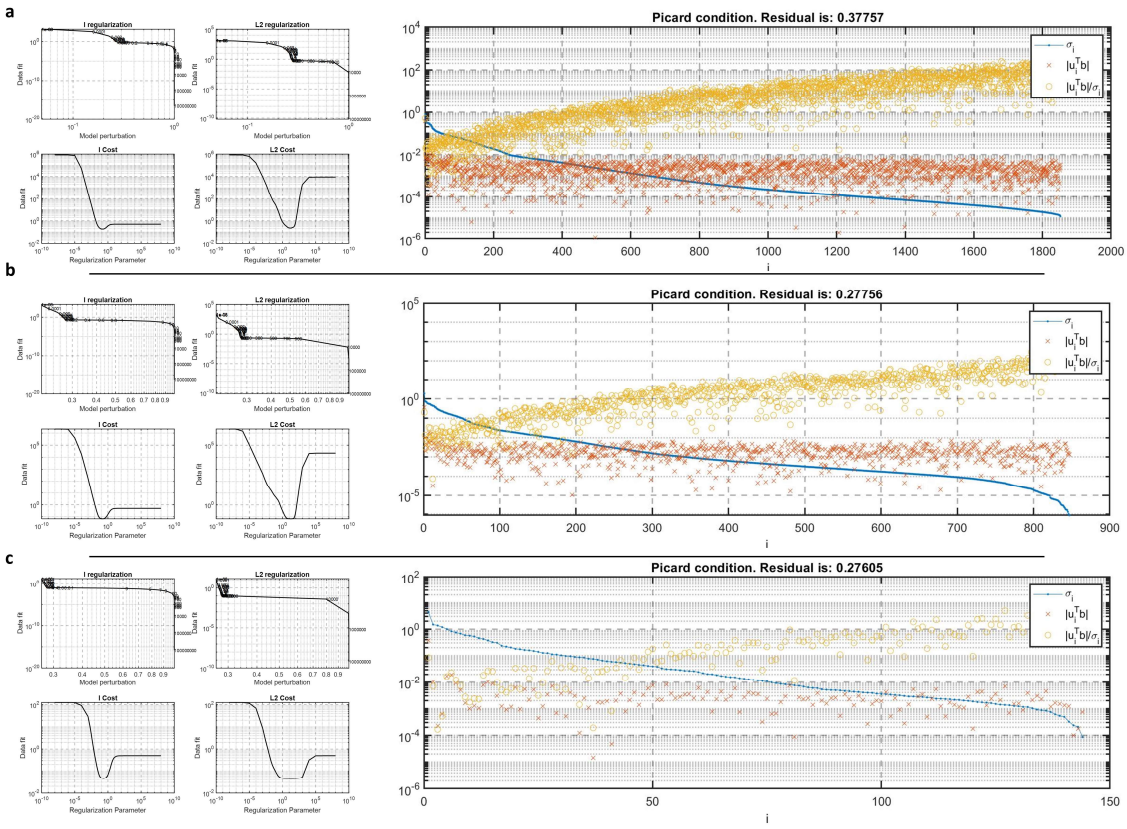

Figure SM-3b. *L-curve (left) and Picard plot (right) for inversion performed at 18 Hz for three different nodes parameterizations:(a)21x21x13; (b) 11x11x7;(c) and 6x6x4 . The results in the manuscript correspond with panel (b). The chosen damping parameters at each frequency are in Table SM-2.*

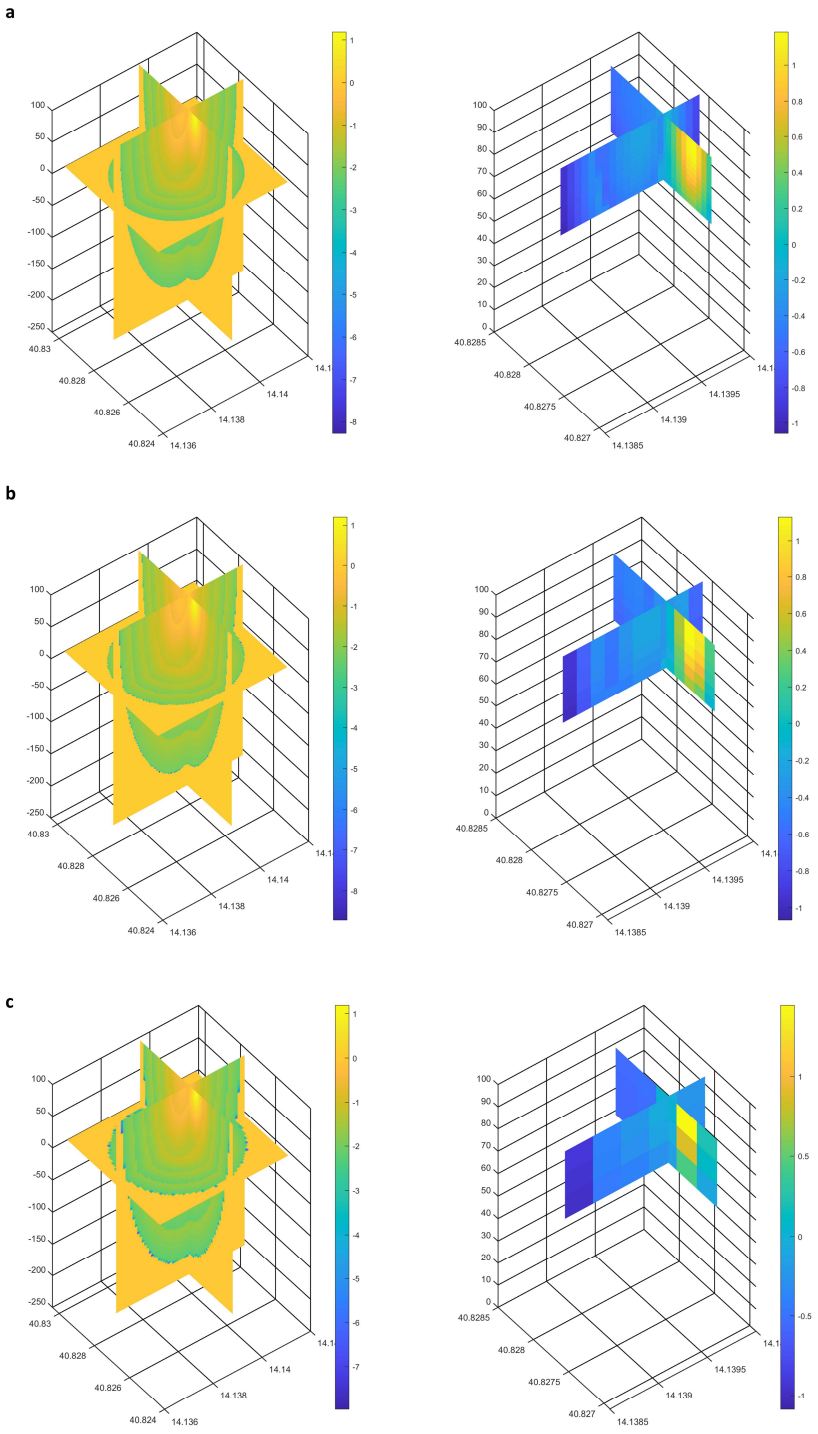

Figure SM-3c. *Sensitivity Kernels for the inversion performed at 18 Hz and three different node parameterizations: (a) 21x21x13;(b) 11x11x7; (c) 6x6x4. The results in the manuscript correspond to panel (b).*